DEFECT AND IMPURITY EFFECTS ON THE INITIAL GROWTH OF Ag ON Si(111)

J.-K. Zuo and J. F. Wendelken

Defect and Impurity Effects On the initial
Growth of Ag On Si(111)

J.-K. Zuo and J. F. Wendelken

Solid State Division, Oak Ridge National Laboratory, Oak Ridge, TN 37831

Abstract

Step and impurity effects on the initial growth of a thin film have been demonstrated in the $(\sqrt{3}\times\sqrt{3})R30°$ domain growth of Ag on Si(111) using high angular resolution LEED. Anisotropy in the $\sqrt{3}$ domain shape and growth during deposition are found on the stepped Si(111) with the preferential growth along the step edge direction. The $\sqrt{3}$ superlattice grows with coverage principally by domain coalescence at the temperature $T \sim 450°C$ and is self-similar at different coverages (scaling) as observed on a flat Si(111). The size distribution is shown to follow a Gamma distribution by a simple model calculation. A dramatic change in the growth mechanism is observed when oxygen impurities (≤ 0.02 ML) appear. The $\sqrt{3}$ domains in the presence of impurities grow with coverage more randomly and isotropically in contrast with the step edge effects and coalescence is inhibited. As a result, the $\sqrt{3}$ superlattice stays in a microdomain morphology without long range order.

I. Introduction

Defects and impurities on a substrate surface often play important roles in the initial stage of epitaxial growth.[1-4] Since adatoms which adsorb at a step defect generally have a larger adsorption energy compared to those which adsorb on a terrace, the steps will generally be preferred sites for adsorption and nucleation. Also, in one-dimensional (1D) migration along a step the probability for an adatom or a cluster to meet another adatom or a cluster is very high. Therefore, the overlayer is expected to grow preferentially along a step edge direction. For randomly distributed impurities, the effects may be in opposition to the step effects. The impurities may attract the adatoms and become nucleation centers in competition with the steps, and they will make the overlayer nucleate and grow more randomly. Further, impurities will trap the domain boundaries, keep the domains from coalescing, and finally break the long-range order of the deposited film. In addition to these effects, impurities may also change some basic growth properties such as the growth law and scaling, which has been observed previously.[3]

In the present paper, we demonstrate these step and impurity effects in the initial growth with Ag/Si(111)($\sqrt{3}\times\sqrt{3}$)R30° as a model system. This system has been extensively studied by almost every surface analysis technique.[5-10] Most work has focused on the determination of atomic geometry of the $\sqrt{3}$ structure, with little attention paid to the $\sqrt{3}$ domain growth. In a separate paper,[11] we reported substrate temperature effects on the $\sqrt{3}$ domain growth as a function of Ag coverage, where the $\sqrt{3}$ structure was found to grow by domain coalescence at high temperature and by small, randomly nucleated domains at low temperature. Also, coverage dependent scaling was observed due to domain coalescence and the growth law was extracted at different temperatures. Here, we report our studies for the step defect and oxygen impurity effects on the $\sqrt{3}$ domain growth using a high angular resolution LEED (HRLEED) system. By analyzing the LEED angular profile associated with the $\sqrt{3}$ structure, we are able to determine the $\sqrt{3}$ domain growth mechanism at the initial stage of Ag deposition on Si(111) in the presence of steps and impurities.

2

II. Experimental

The experiments were performed in a UHV chamber containing HRLEED, Auger Electron Spectroscopy (AES) with a double-pass cylindrical mirror analyzer, an Ag evaporation source, and a gas handling system providing various high purity (6N) gases. Pressures were routinely in the 10^{-11} Torr range. The HRLEED (or Spot-Profile-Analysis LEED[12]) is controlled by a personal computer and has a spatial resolution $\leq 6 \times 10^{-3}$ Å^{-1} in k-space. A good signal-to-noise ratio is obtained by using a channeltron detector. These features allow us to record the angular profile of any diffraction beam accurately and quickly, so that the evolution of the ordered domains can be determined.

The Si samples with size ~ 0.9×0.9 cm^2 were cut from a n-type Si(111) wafer. The misorientation from (111) was less than $0.2°$. The sample was mounted in a Mo housing in which the sample could be heated or cooled below room temperature. Temperature was measured by a W5%Re-W26%Re thermocouple in contact with a corner of the sample. The Si(111) sample was first annealed at ~ 1200 °C to remove the oxide layer and carbon impurities. Later, to desorb Ag overlayers and oxygen impurities from the substrate and restore the clean Si(111)7×7 surface, the sample usually was annealed at ~ 900–1000°C. After the annealing, no contamination was detectable with AES and the clean Si(111) surface exhibited a sharp 7×7 LEED pattern. Ag atoms were evaporated at a fixed rate of ~ 0.15 ML/min from a pure (5N) Ag foil heated by electron bombardment from the backside. We found that this evaporation method can produce a contamination free Ag deposition within our AES detection limit. Oxygen impurities and Ag coverage were estimated using AES and the total intensity measurement of a $\sqrt{3}$ superlattice LEED beam as described in detail elsewhere.[11]

III. Step Effects On the $\sqrt{3}$ Domain Growth

The step density on the Si(111) surface was characterized by measuring the FWHMs of both the (00) and (1/7 0) beams. The FWHM of the (00) beam at an out-of-phase condition, e.g. an incident electron energy E=78 eV, is inversely proportional to the average terrace width and the

3

FWHM of the (1/7 0) beam is inversely proportional to the diameter of the average 7×7 ordered region which was found to be equal to the average terrace size. For the "flat" Si(111) surface, the average terrace width is estimated to be ≥ 1000 Å in all directions, which is our instrument resolution limit. The step defects were created by heating the sample to ~ 1200–1300 °C many times.[13] After this heat treatment, we estimate that the average terrace width is still ~ 1000 Å along the $[\bar{2}11]$ (step edge) direction but is reduced to ~ 550 Å along the $[0\bar{1}1]$ direction. At the same time mosaic structures with small mosaic angles were created in the $[0\bar{1}1]$ direction during the heat treatment.

When a submonolayer of Ag is deposited on the Si(111)7×7 surface above ~ 200 °C, a $\sqrt{3}$ superlattice forms which is detectable at less than 0.1 ML. In our temperature dependent study,[11] we have learned that with increasing coverage, the $\sqrt{3}$ superlattice grows more perfectly at higher substrate temperature than at lower temperature. Thus, to see the step and impurity effects, it is better to choose a high temperature (T ~ 450°C) as the deposition condition. In our measurements, we have collected the angular profiles of the (1/3 1/3) beam as a function of Ag coverage (θ) since the angular profile of any superlattice diffraction beam depends solely on the domain size distribution. The depositions were performed at T = 450°C and the LEED measurements were done after the sample cooled to near room temperature. The domain morphology at high deposition temperature may be frozen out when the sample is cooled to room temperature. Figure 1(a) and (b) show the full width at the half maximum (FWHM) of the (1/3 1/3) beam vs Ag coverage scanned in the $[\bar{1}\bar{1}2]$ and $[\bar{2}11]$ directions, respectively, for the flat and stepped Si(111) surfaces as well as for two different oxygen impurity doped cases. The oxygen doped cases will be discussed in the next section. We did not measure the angular profile in the $[0\bar{1}1]$ direction which is perpendicular to the step edge along the $[\bar{2}11]$ direction, but instead measured that in the $[\bar{1}\bar{1}2]$ which is 30° from the $[0\bar{1}1]$. Since the FWHM of any $\sqrt{3}$ superlattice beam is inversely proportional to average domain size in a specific direction, from Fig. 1 we can see that in the $[\bar{1}\bar{1}2]$ the $\sqrt{3}$ domain size on the stepped Si(111) becomes smaller than that (dashed curves) on the flat one after $\theta \sim 0.5$ ML, but in the $[\bar{2}11]$ direction the situation is just the opposite, i.e., the domain

size on the stepped surface is much larger for all coverages. Also, the domain size in the step edge direction is already quite big even at low coverage as indicated by the narrow FWHM. This tells us that on the stepped surface the Ag atoms may be easily captured at steps and the $\sqrt{3}$ domains preferentially grow along the step edge direction. More interestingly, we found that the ratio of the FWHM in the $[\bar{2}11]$ to that in the $[\bar{1}\bar{1}2]$ does not change with coverage but changes when steps appear. For the flat Si(111), this ratio (after removing the instrument response width) is ~ 0.90 ± 0.03 indicating a nearly round domain shape, and it changes to ~ 0.56 ± 0.02 for the stepped surface on which the domains are elongated along the step edge. The domain shapes are determined by several factors. The domain-domain interaction promotes round domains, but the domain-step interaction forces the domains to elongate in the step edge direction. Thus, the invariant domain shape at different coverages on either the flat or stepped surface should be a result of the balance of all these interactions.

This anisotropic growth on the stepped surface is also reflected in the growth law which describes the average domain size as a function of coverage. In Fig. 2(a) and (b) we have plotted 1/FWHM of the (1/3 1/3) beam vs θ in a ln-ln scale for the flat and stepped Si(111) surfaces, where the instrument response width has been removed. As seen in the figures, a power growth law can be established via

$$\bar{N} \propto \frac{1}{FWHM} \propto \theta^n . \tag{1}$$

For the flat surface, the growth exponent n is fit to be 0.35 and 0.36 ± 0.02 in the $[\bar{2}11]$ and $[\bar{1}\bar{1}2]$ directions, respectively. The similar n indicates an isotropic growth on the flat surface. However, n has different values of 0.42 ± 0.03 and 0.27 ± 0.02 in the $[\bar{2}11]$ and $[\bar{1}\bar{1}2]$, respectively, for the stepped surface. As compared with the flat Si(111) case, the fact that n is enhanced along the step edge and lowered in the $[\bar{1}\bar{1}2]$ implies that the preferential growth along the step edge is at the expense of the growth in other directions.

In addition to the above information, it is frequently desirable to know the domain size distribution as a function of coverage at a fixed deposition rate and substrate temperature to gain insight into additional details of the growth mechanism. The domain size distribution can in principle be extracted from the angular profile as long as an appropriate model can be established. The model used here assumes that the positions of domain boundaries are randomly distributed so that the interference between domains is negligible.[14] The intensity of any superlattice beam are then the sum of the intensities diffracted from individual domains,[14] i.e.,

$$I(S,\theta) = \sum_{N=1}^{\infty} P(N,\theta) \ \frac{\sin^2 \frac{N}{2} (S_{||} \cdot a)}{\sin^2 \frac{1}{2} (S_{||} \cdot a)} \ ,$$ (2)

where the weight $P(N,\theta)$ is the size distribution function describing the probability of finding a domain with N lattice spacings at a coverage θ, $S_{||}$ and a are the momentum transfer parallel to the surface and the lattice constant (6.65 Å) of the $\sqrt{3}$ structure, respectively. This assumption should hold well for a system with the ground state degeneracy $Q > 2$ because the larger the Q, the more complicated and random domain boundary structure could be. The Q for the $\sqrt{3}$ structure of the Ag/Si(111) with the honeycomb arrangement[5] is larger than 3, therefore the model should be suitable for our case, especially for the impurity doped cases. For comparison with the experiment, a distribution function $P(N,\theta)$ can be chosen and $I(S,\theta)$ evaluated using Eq. (2). $I(S,\theta)$ is then convoluted with the instrument response function to fit the measured profiles. We have tried several distributions including Gaussian, geometric, Raleigh and Gamma distributions, and found that the Gamma distribution has the best fit. The fit of the Raleigh distribution is slightly worse than that of the Gamma distribution. The Gamma distribution has the form:

$$P(N,\theta) = \frac{1}{\lambda^{\alpha} \Gamma(\alpha)} \ N^{\alpha-1} e^{-N/\lambda} \ ,$$ (3)

6

with the mean $\bar{N} = \alpha\lambda$ and distribution width $\sigma \equiv \sqrt{(N-\bar{N})^2} = \lambda\sqrt{\alpha}$, where α and λ were chosen as fitting parameters which are functions of θ and T. Figure 3(a) shows the angular profiles of the $(1/3\ 1/3)$ beam at different coverages in the $[\bar{1}\bar{1}2]$ direction from the stepped Si(111). The solid curves in the figure are the least-square fits obtained utilizing the Gamma distribution in Eq. (2) convoluted with the instrument response function. The best fits at different coverages all give $\alpha = 3.3 \pm 0.3$, with λ increasing considerably from 7.6 to 23.1 for $\theta \sim 0.05$ to 1 ML. The corresponding mean size $\bar{N}$ is calculated to be 24.3 to 69.3 lattice spacings. A similar fit is also obtained in the $[\bar{2}11]$ direction where the best fit for α is 3.5 ± 0.3 and λ increases from 10.3 to 28.7 for $\theta \sim 0.05$ to 1 ML. The mean size is calculated to be 35.0 to 97.7. In addition, the width ratio of the $\bar{N}$ in the $[\bar{1}\bar{1}2]$ to that in the $[\bar{2}11]$ is ~ 0.7 which is larger than that (~ 0.56) directly evaluated from the FWHM of the profile. Similar behavior is also found in the flat surface and impurity doped cases. The difference from the FWHM evaluation may be due to the underestimate of the domain size in this incoherent scattering model, especially in the $[\bar{2}11]$ direction in which the profile usually is narrower than in the $[\bar{1}\bar{1}2]$ direction. Shown in Fig. 3(b) and (c) are the evolution of the corresponding size distributions obtained from the best fits. From these figures we can gain an insight into three things. First, the dramatic increase of the mean and width in the distribution with coverage indicates that the growth is governed by domain coalescence at the substrate temperature T = 450°C. Also, the coalescence occurs more rapidly in the $[\bar{2}11]$ than in the $[\bar{1}\bar{1}2]$ direction due to step effects. Second, when the parameter $\alpha > 1$ just as in our case, the Gamma distribution will peak at $N_p = (\alpha-1)\lambda$. The steeper slope of the distribution for $N < N_p$ than that for $N > N_p$ indicates that the probability of finding a domain with size N decreases much faster for $N < N_p$ than for $N > N_p$ where it decays exponentially. Thus, the interactions among the domain boundaries are strong in the $N \ll N_p$ region and become negligible in the $N \gg N_p$ region.[15] Therefore, the boundary interactions in our system are a short-range interaction with a range of $\sim N_p a$.[15] Third, and more interesting, since the growth is governed by domain coalescence, one expects the existence of scaling, i.e., self-similar growth, in the growth process because

7

coalescence simply rescales length but leaves the basic morphology of domains unchanged.[16] Indeed, the Gamma distribution in Eq. (3) with a fixed α can be expressed in a scaling form:

$$P(N,\theta) = \frac{1}{\alpha\lambda}\frac{\alpha^\alpha}{\Gamma(\alpha)}\left(\frac{N}{\alpha\lambda}\right)^{\alpha-1}e^{-\alpha(N/\alpha\lambda)} = \frac{1}{\bar{N}(\theta)}P'(x) , \qquad (4)$$

where $x = N/\bar{N}$ ($\bar{N}=\alpha\lambda$) and $P'(x) = \{\alpha^\alpha/\Gamma(\alpha)\}x^{\alpha-1}e^{-\alpha x}$ is a scaling function independent of coverage θ. In other words, although the mean size varies with coverage, the functional form of the size distribution does not. According to Eq. (4), we have replotted $P'(x) \equiv \bar{N}P(N,\theta)$ vs x in the inset of Fig. 3(b) and (c). Remarkably, although $P(N,\theta)$ broadens with coverage θ, the $P'(x)$ superpose on each other independent of coverage. This coverage dependent scaling is also observed for the growth on the flat Si(111) surface.[11]

To confirm the existence of scaling, we have tested it in another way where a power Lorentzian,

$$I(S) = \frac{A}{(S_\parallel^2 + \kappa^2)^m} , \qquad (5)$$

convoluted with the instrument response function is used to fit the angular profiles of the (1/3 1/3) beam at different coverages. The inverse correlation length κ and exponent m are the fitting parameters, and A is a constant. We found that Eq. (5) can describe the measured profiles very well with $m = 1.5 \pm 0.1$ and κ varying with coverage. The fits are shown in the dashed lines in Fig. 3(a) which are essentially indistinguishable from those of Eq. (2) using the Gamma distribution. That the same value of m was obtained for different coverages implies that the angular profile I(S) also contains a scaling function, $I'(x') = 1/(1+x'^2)^m$ with $x'= S_\parallel/\kappa$. Since the angular profile uniquely reflects the size distribution, it again proves the existence of scaling in the coverage dependent growth.

IV. Impurity Effects On the $\sqrt{3}$ Domain Growth

In the study of impurity effects, the oxygen was chosen as the impurity because oxygen is easily removed to repeat the experiment and is also a common contaminant (SiO_2) on the Si surfaces. The experiments were all performed on the stepped Si(111) surface. In the experiment, a small amount (≤ 0.02 ML) of oxygen was adsorbed on the clean Si(111)7x7 at room temperature before the Ag deposition, and the dose was examined by AES with a relative uncertainty of ~ 0.3 % ML. After the oxygen doping, the 1/7-order beams were almost unchanged. In Fig. 1(a) and (b) the FWHM of the (1/3 1/3) beam vs Ag coverage for the two different oxygen doses are shown in comparison with those for the clean case. As we can see, for any θ the FWHM broadens with increasing oxygen dose, indicating that the greater the impurity dose, the smaller the $\sqrt{3}$ domains. Also, the ratio of the FWHM in the [$\bar{2}11$] to that in the [$\bar{1}\bar{1}2$] increases from ~ 0.56 for the pure case. For the oxygen dose of ~ 0.01 ML the ratio is 0.75 ± 0.03 at all Ag coverages, and for the oxygen dose of ~ 0.02 ML it varies from ~ 0.75 to ~ 0.88 for an Ag coverage of θ ~ 0.1 to 1 ML. Obviously, the impurities make the $\sqrt{3}$ domains nucleate and grow more randomly and isotropically in competition with the step influence. This may be seen more clearly in Fig. 4 where 1/FWHM vs Ag coverage is plotted in a ln-ln scale for the oxygen dose of ~ 0.02 ML. A power law growth of $\bar{N}$ with Ag coverage only holds before ~ 0.6 ML, and after that it almost levels off This indicates that the impurities tend to block the growth when the $\sqrt{3}$ domains grow to a certain size (~ 29 lattice spacings fit by Eq. (2) using the Gamma distribution) at the Ag coverage of ~ 0.6 ML. According to Eq. (1) and fitting to the linear slope, the growth exponent n is extracted to be ~ 0.35 in the [$\bar{1}\bar{1}2$] and ~ 0.31 in the [$\bar{2}11$] direction. The values of n in the two directions now become closer as compared with those for the stepped surface with no impurities, implying the dominant effects of the impurities over the steps. The slightly smaller value of n in the [$\bar{2}11$] direction might be due to the preferential distribution of the oxygen impurities in the [$\bar{2}$)11] step edge direction.

In order to see the size distribution in the presence of the oxygen impurities, we have fit Eq.

(2), using the Gamma size distribution and convoluted with the instrument response function, to

the angular profiles for the oxygen doped cases. Shown in Fig. 5(a) and (b) are the angular

profiles in the $[\bar{1}\bar{1}2]$ and $[\bar{2}11]$ directions, respectively, at different Ag coverages for the oxygen

dose of ~ 0.02 ML. The fits (solid curves) are found to be excellent and the best fit size

distributions at different coverages are shown in Fig. 6. The corresponding parameters of α and λ

are 4.4 ± 0.3 and 3.7 to 7.6 in the $[\bar{1}\bar{1}2]$, and 2.2 ± 0.2 and 7.8 to 13.3 in the $[\bar{2}11]$ direction,

respectively, for a Ag coverage of ~ 0.1 to 1 ML. In contrast to the growth on the clean Si(111) at

the same temperature (T = 450°C), the size distribution now is much narrower and changes little

with coverage, which is quite similar to the growth on the flat and clean Si(111) at low

temperature.[11] This clearly demonstrates that the impurities will not only make the $\sqrt{3}$ domains

nucleate randomly but also tends to prevent domain coalescence and break the long range order in

the thin film growth. The difference in α for the two directions means some difference in the size

distributions. In the Gamma distribution, a smaller α implies weaker interactions among the

domain boundaries. When α reduces to 1 the Gamma distribution becomes the exponential

distribution, the continuum limit of the geometric distribution, which implies a totally random

distribution of the domain boundaries and a negligible boundary-boundary interaction.[15,17]

Therefore, the smaller α in the $[\bar{2}11]$ may be attributed to more roughening of the boundary

structure in this direction than in the $[\bar{1}\bar{1}2]$. The impurity-induced roughening at domain

boundaries usually will be energetically favored and reduce the boundary-boundary interactions.[2]

Finally, the mean size $\bar{N}$, expressed in lattice spacings, at a Ag coverage from ~ 0.1 to 1 ML are

calculated to be ~ 16 to 55 in the $[\bar{2}11]$ and ~ 15 to 50 in the $[\bar{1}\bar{1}2]$ for an oxygen dose of ~ 0.01

ML, and ~ 15 to 31 in both the directions for an oxygen dose of ~ 0.02 ML. The size decreases

with increasing oxygen dose and is much smaller than that grown on the surface with no

impurities.

V. Conclusions

We have presented HRLEED data on step and impurity effects on the coverage dependent $\sqrt{3}$ domain growth of Ag on Si(111). On the stepped Si(111), an anisotropic growth and shape in the $\sqrt{3}$ domain are found with the preferential growth along the step edge direction. The growth is governed by domain coalescence at T ~ 450°C as indicated by the considerable increase in the mean and width of the size distribution, and is self similar (scaling) at different coverages as a result of the coalescence. The size distribution is consistent with a Gamma distribution as determined by a comparison of a simple model calculation to the angular profile of a $\sqrt{3}$ diffraction beam. In the presence of oxygen impurities (≤ 0.02 ML), the anisotropy in the $\sqrt{3}$ domain shape diminishes with increasing oxygen dose, and the domains nucleate and grow more randomly and isotropically. Also, the impurities block domain coalescence and break the long range order in the $\sqrt{3}$ structure.

References

1. B. Lewis and J. C. Anderson, *Nucleation and Growth of Thin Films* (Academic, New York, 1978).

2. G. S. Grest and D. J. Srolovitz, *Phys. Rev. B* **32**, 3014 (1985); ibid. 3021 (1985); D. A.Huse and C. L. Henley, *Phys. Rev. Lett.* **54**, 2708 (1985); Y. Imry and S.-K. Ma, *Phys. Rev. Lett.* **35**, 1399 (1975).

3. J.-K. Zuo, G.-C. Wang, and T.-M. Lu, *Phys. Rev. B* **40**, 524 (1989).

4. Y. Gotch, S. Ino, and H. Komatsu, *J. Cryst. Growth* **56**, 498 (1982).

5. E. J. Van Loenen, J. E. Demuth, R. M. Tromp, and R. J. Hamers, *Phys. Rev. Lett.* **58**, 373 (1987); R. J. Wilson and S. Chiang, *Phys. Rev. Lett.* **58**, 369 (1987); ibid. **59**, 2329 (19^"'

6. Y. Horio and A. Ichimiya, *Surf. Sci.* **164**, 589 (1985).

7. T. L. Porter, C. S. Chang, and I. S. I. Tsong, *Phys. Rev. Lett.* **60**, 1739 (1988).

8. M. Saiton, F. Shoji, K. Oura, and T. Hanawa, *Surf. Sci.* **112**, 306 (1981); J.Stohr, R. Jaeger, G. Rossi, T. Kendelewicz, and I. Lindau, *Surf. Sci.* **134**, 813 (1983); S. Kono, K. Higashiyama, and T. Sagawa, *Surf. Sci.* **165**, 21 (1986).

9. E. L. Bullock, G. S. Herman, M. Yamada, D. J. Friedman, and C. S. Fadley, *Phys. Rev. B* **41**, 1703 (1990).

10. Takahashi, S. Nakatani, N. Okamoto, T. Ishikawa, and S. Kikuta, *Jpn. J. Appl. Phys.* **27**, L753 (1988).

11. J.-K. Zuo and J. F. Wendelken, in preparation.

12. U. Scheithauer, G. Mayer, and M. Henzler, *Surf. Sci.* **178**, 441 (1986).

13. J.-K. Zuo, R. A. Harper, and G.-C. Wang, *Appl. Phys. Lett.* **51**, 250 (1987).

14. T.-M. Lu, L.-H. Zhao, M. G. Lagally, G.-C. Wang, and J. E. Houston, *Surf. Sci.* **122**, 519 (1982).

15. J. M. Pimbley and T.-M. Lu, *Surf. Sci.* **159**, 169 (1985); *J. Appl. Phys.* **58**, 2184 (1985).

16. D. Beysens and C. M. Knobler, *Phys. Rev. Lett.* **57**, 1433 (1986).

17. T.-M. Lu and M. G. Lagally, *Surf.Sci.* **120**, 47 (1982); J. M. Pimbley, T.-M. Lu, and G.-C. Wang, *Surf. Sci.* **159**, L467 (1985).

Figure captions

Fig. 1   The FWHM of the (1/3 1/3) diffraction beam as a function of Ag coverage (raw data) in
(a) the $[\bar{1}\bar{1}2]$ and (b) the $[\bar{2}11]$. The deposition temperature T = 450°C and the incident
electron energy E = 84 eV.

Fig. 2   The ln-ln plot of 1/FWHM vs Ag coverage for the (1/3 1/3) beam for (a) the flat and (b)
the stepped Si(111) surfaces. The deposition temperature T = 450°C and the instrument
response width has been removed.

Fig. 3   (a) The angular profiles of the (1/3 1/3) beam at different coverages measured from the
stepped Si(111). The solid curves are the best fits of Eq. (2) using the Gamma
distribution. The dashed curves are the best fits of the power Lorentzian in Eq. (5) which
are nearly indistinguishable from the solid curves. (b) and (c) The evolution of the
Gamma size distribution with coverage in the $[\bar{1}\bar{1}2]$ and $[\bar{2}11]$ directions, respectively,
obtained using the fitting in (a). The insets in (b) and (c) are the corresponding scaling
functions P'(x) vs x.

Fig. 4   The ln-ln plot of 1/FWHM vs Ag coverage for the (1/3 1/3) beam for the oxygen dose of
~ 0.02 ML. The instrument response width has been removed.

Fig. 5   The angular profiles of the (1/3 1/3) beam at different Ag coverages in (a) the $[\bar{1}\bar{1}2]$ and
(b) the $[\bar{2}11]$ directions for the oxygen dose of ~ 0.02 ML. The solid curves are the best
fits of Eq. (2) using the Gamma distribution.

Fig. 6   The evolution of the size distribution with Ag coverage obtained by the fits in Fig. 5(a)
and (b) for T = 450°C.

Fig.1

Fig. 2
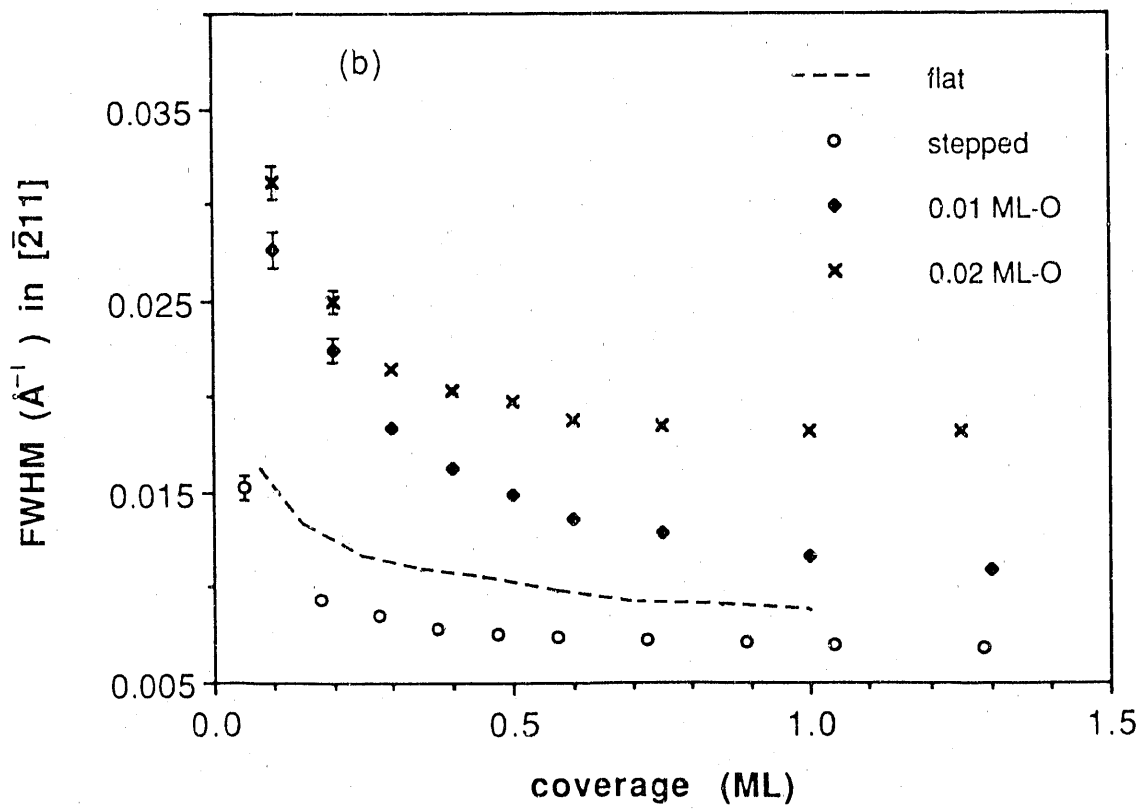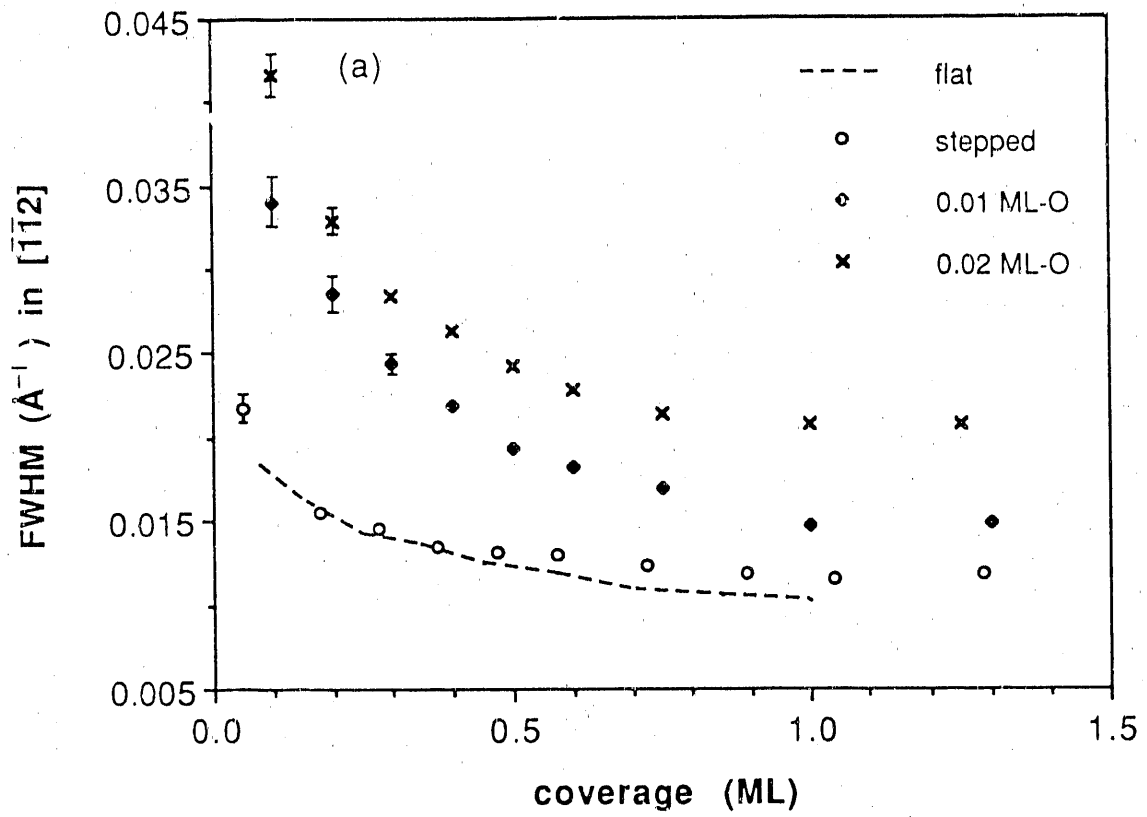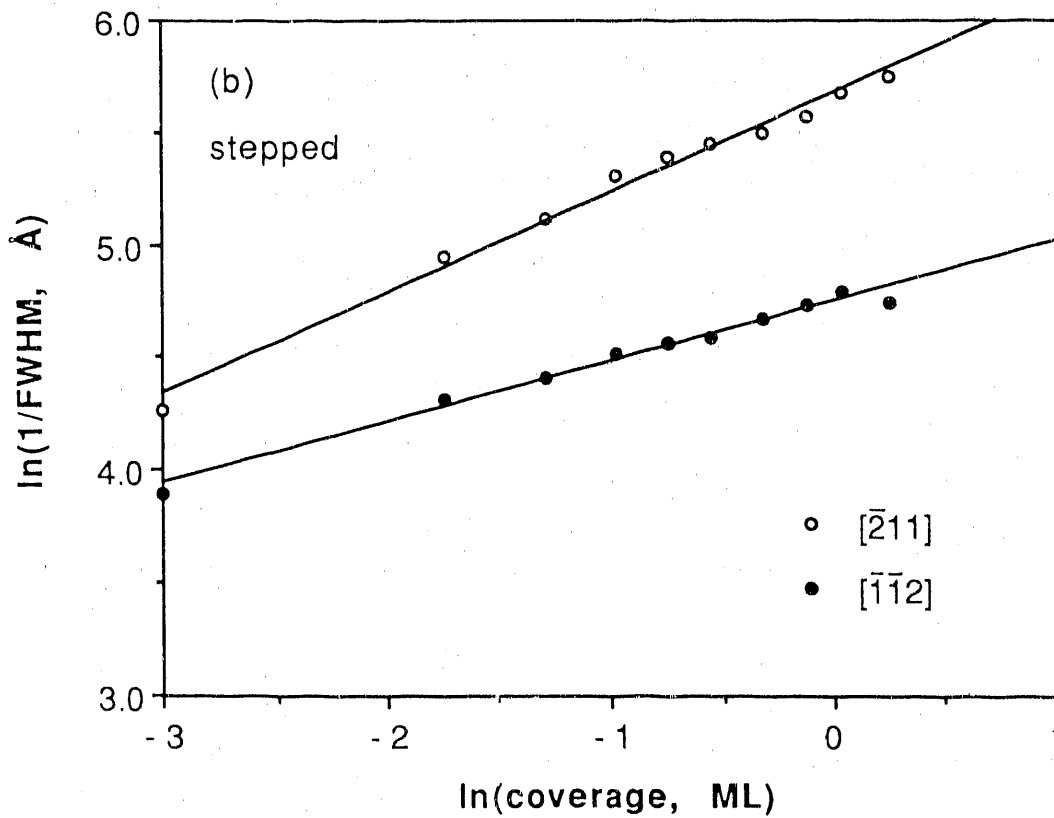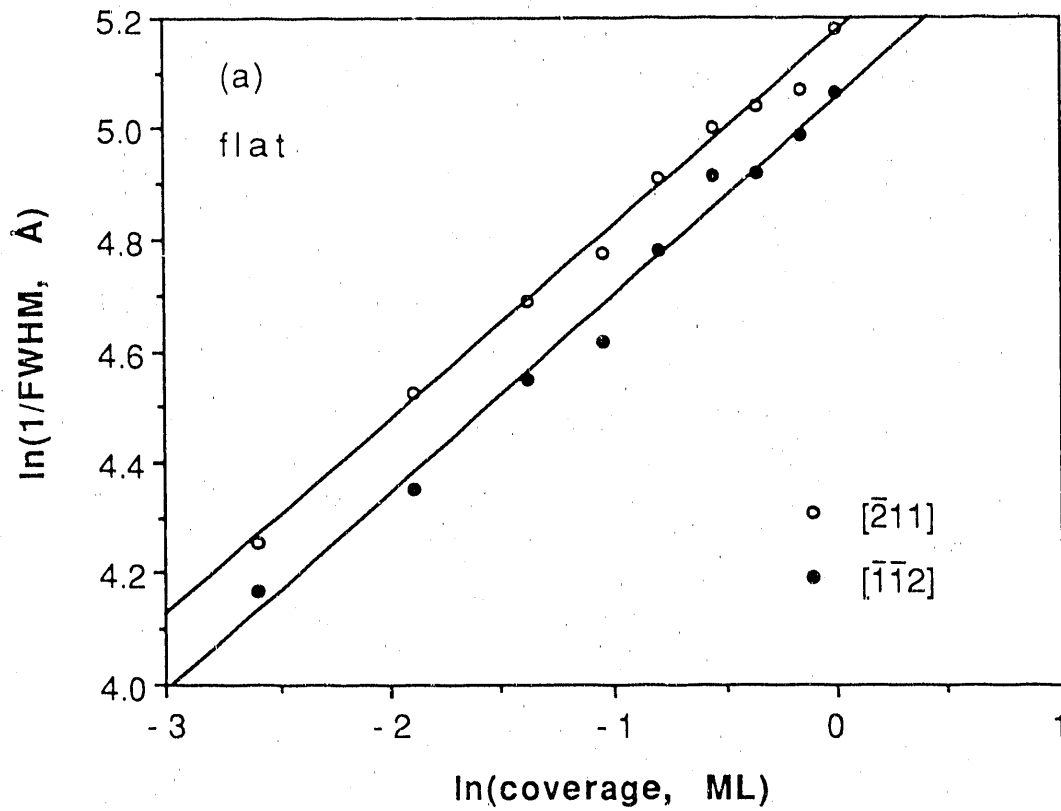
Fig. 3(a)

Fig. 3(b)

(b)

in [$\bar{1}1\bar{2}$]

$P'(x)$

x

$P(N,\theta) \times 10^{-3}$

0.05 ML

0.18 ML

0.38 ML

0.73 ML

1.00 ML

N, lattice spacings of $\sqrt{3}$ domain
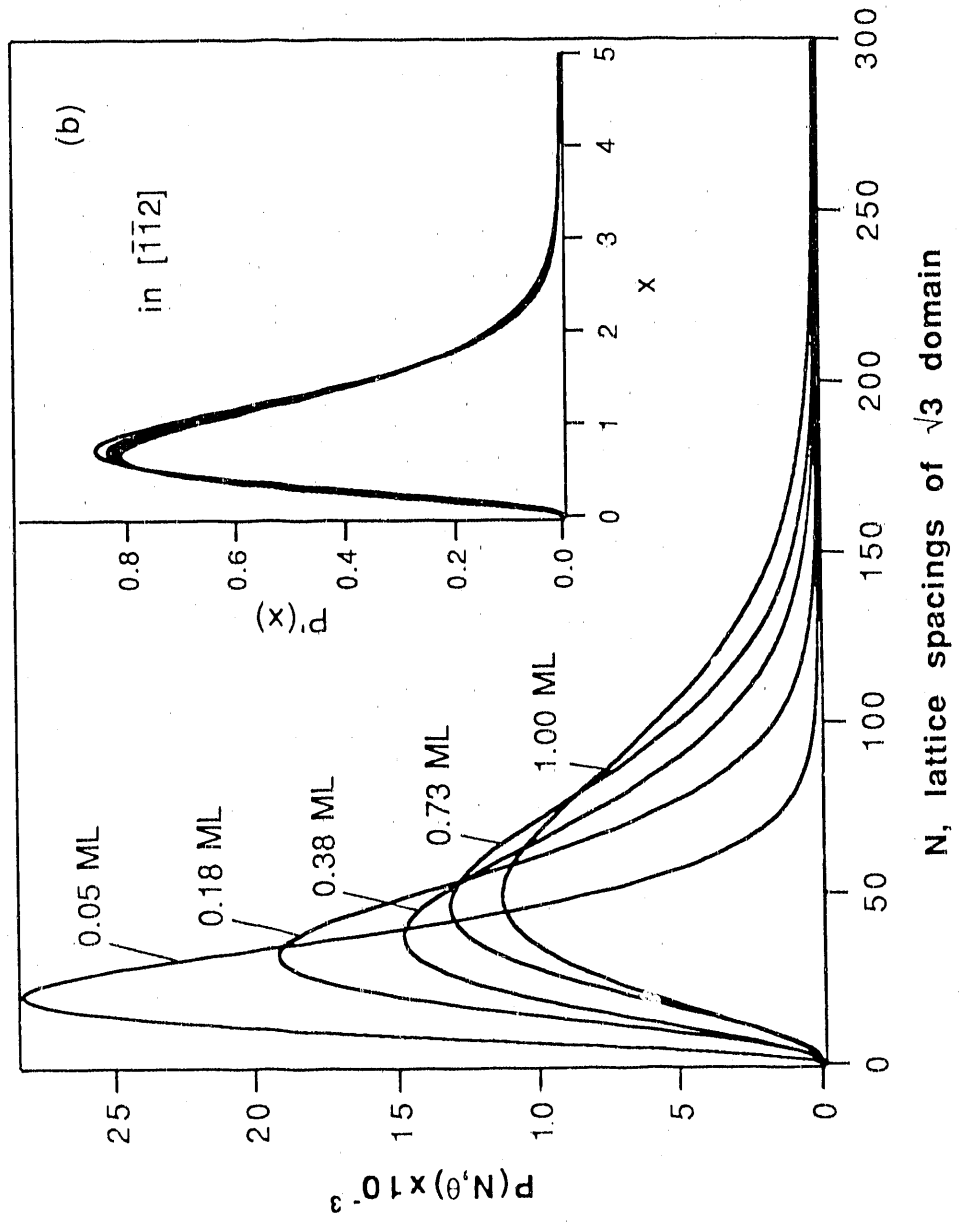
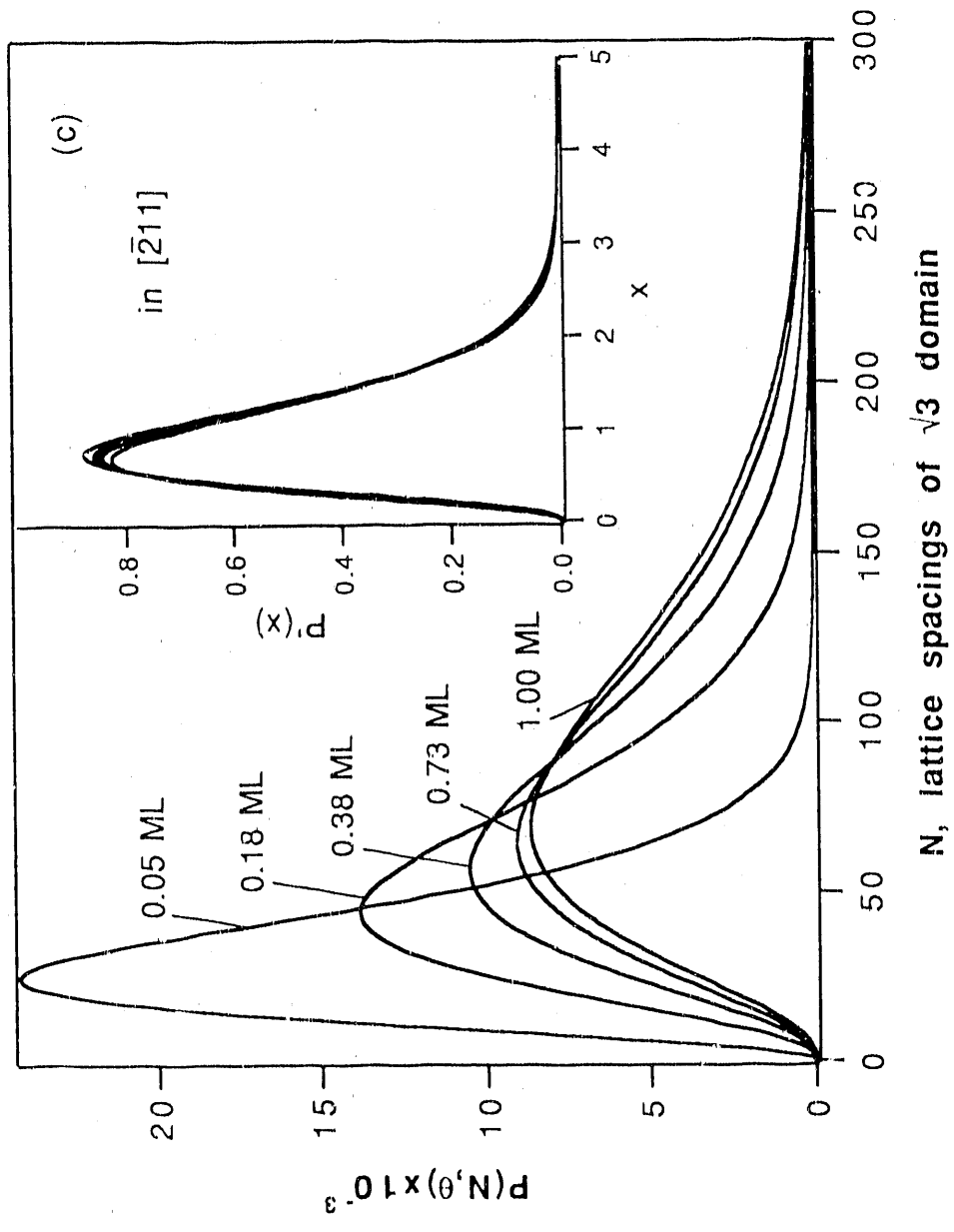Fig. 3(c)

Fig. 4

Fig. 5(a)

(b)

θ (ML):

0.10 ML
0.20 ML
0.40 ML
0.60 ML
1.00 ML

0.02 ML-O
T = 450°C
[2̄11] scan

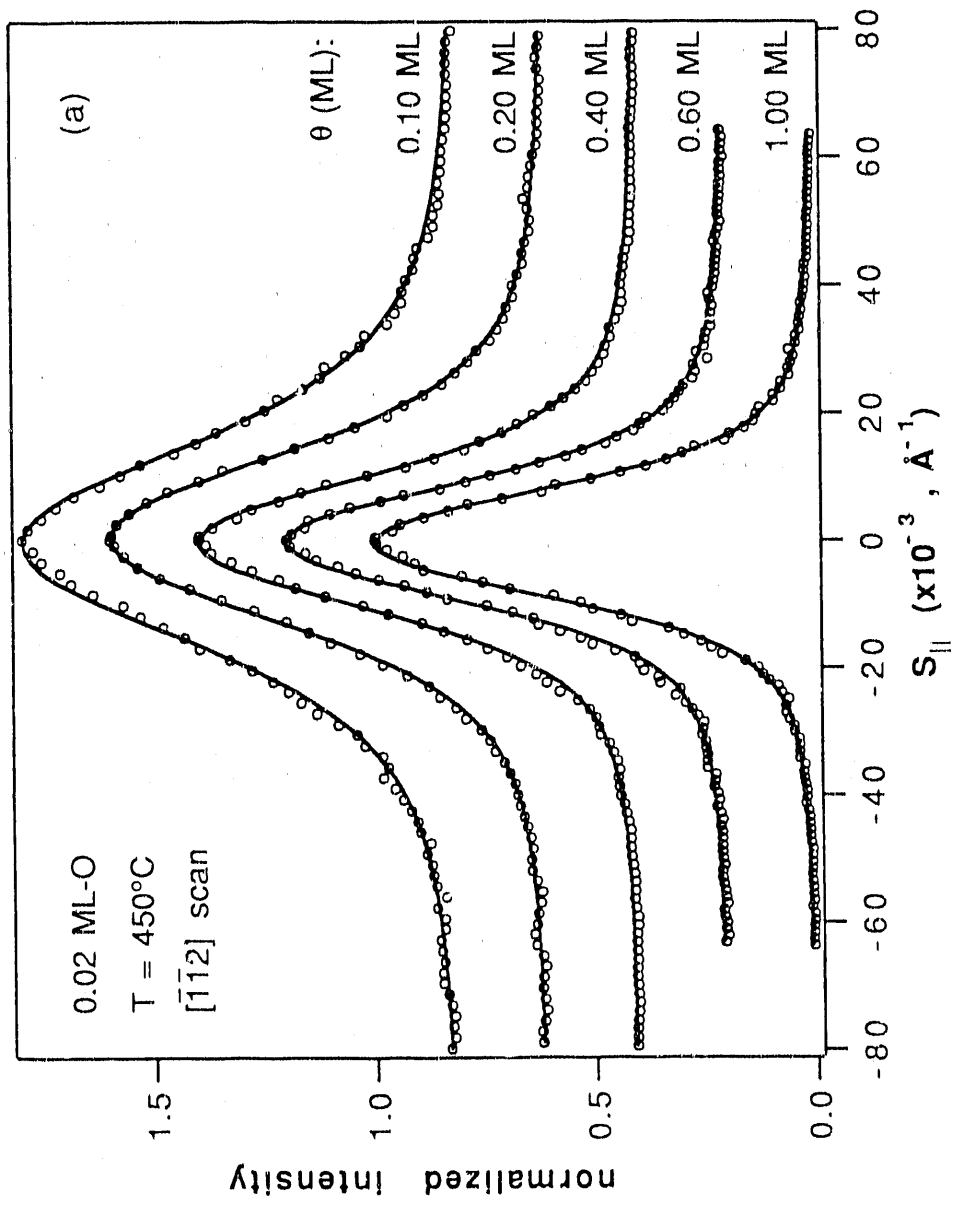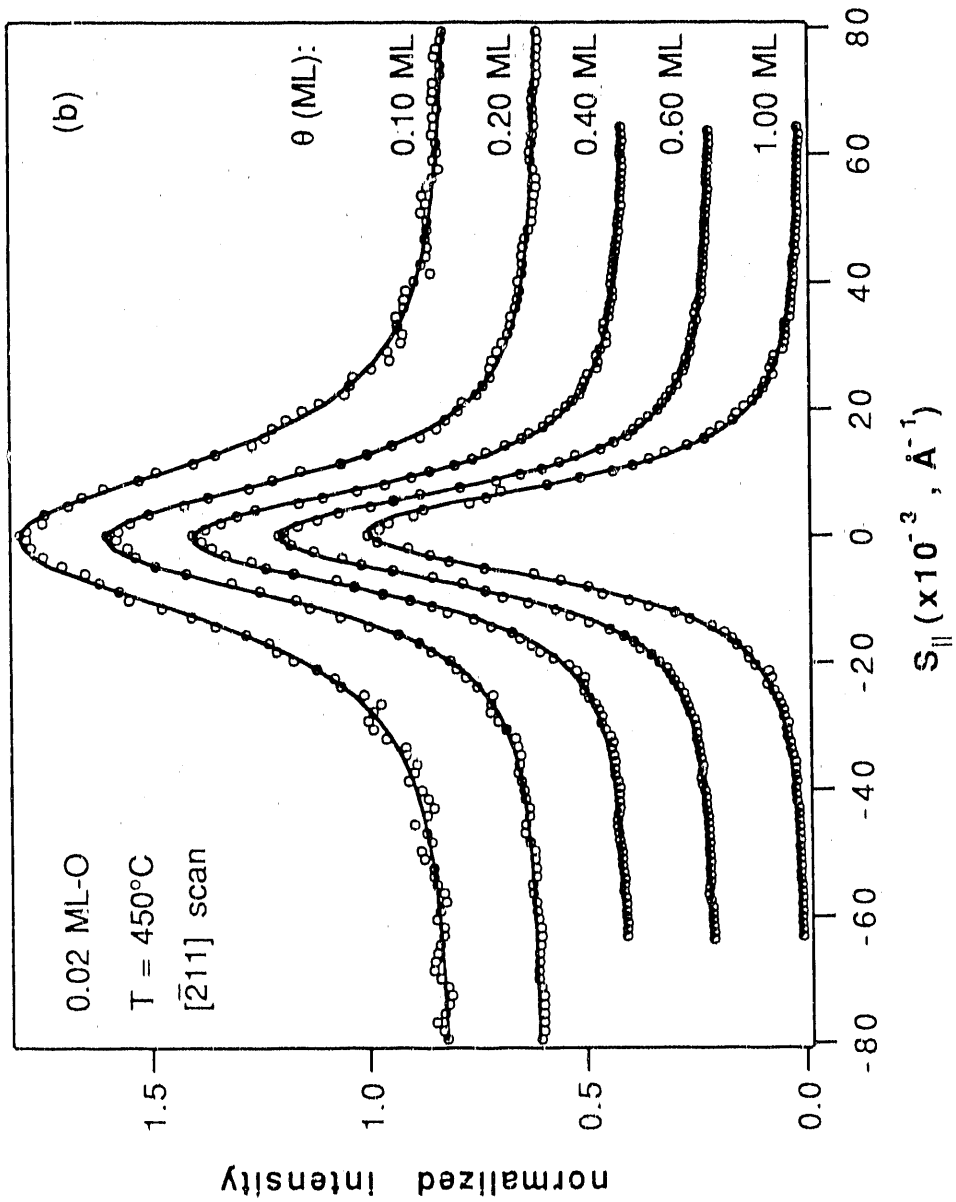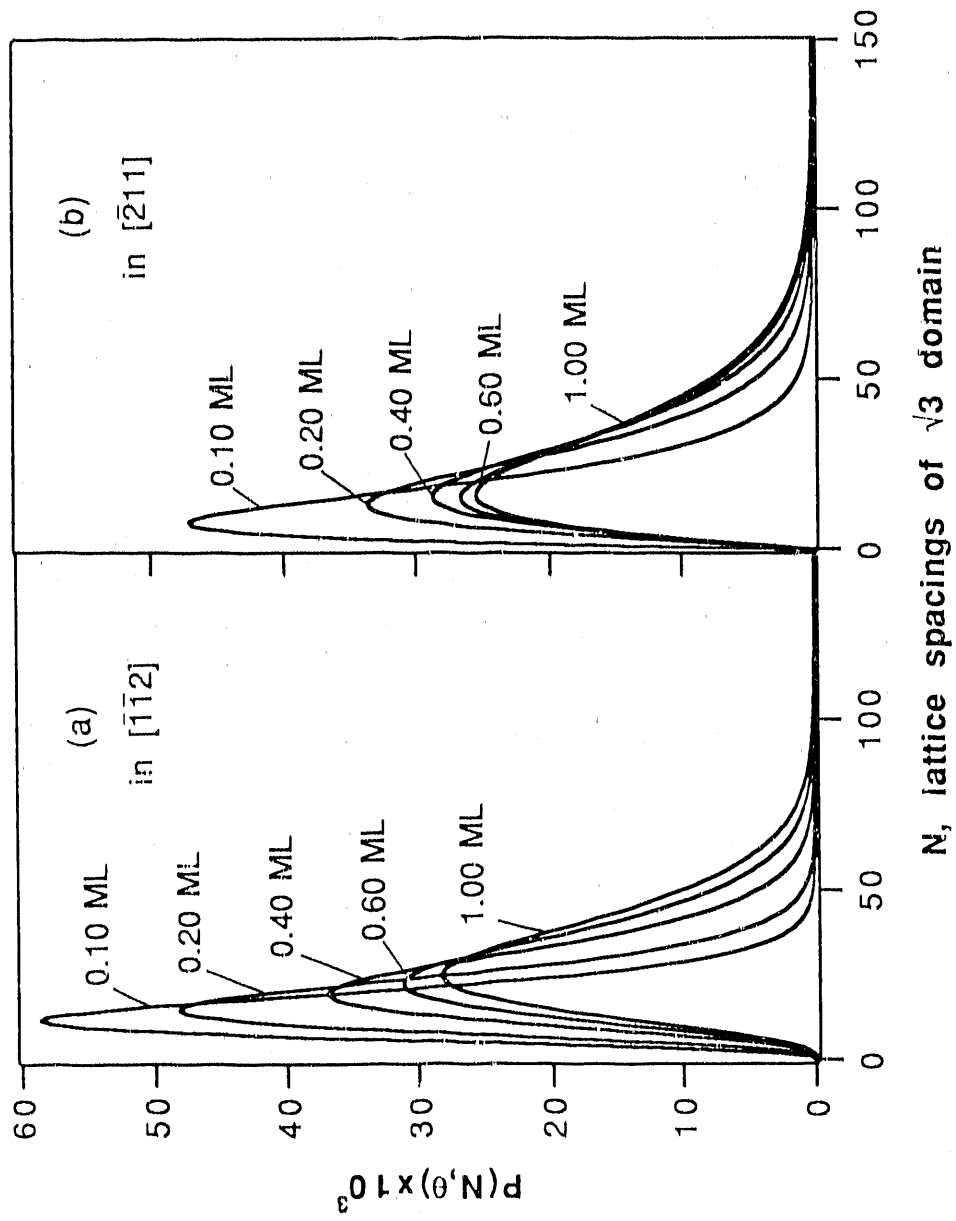normalized intensity

$S_{\parallel}$ ($\times 10^{-3}$, Å^{-1})
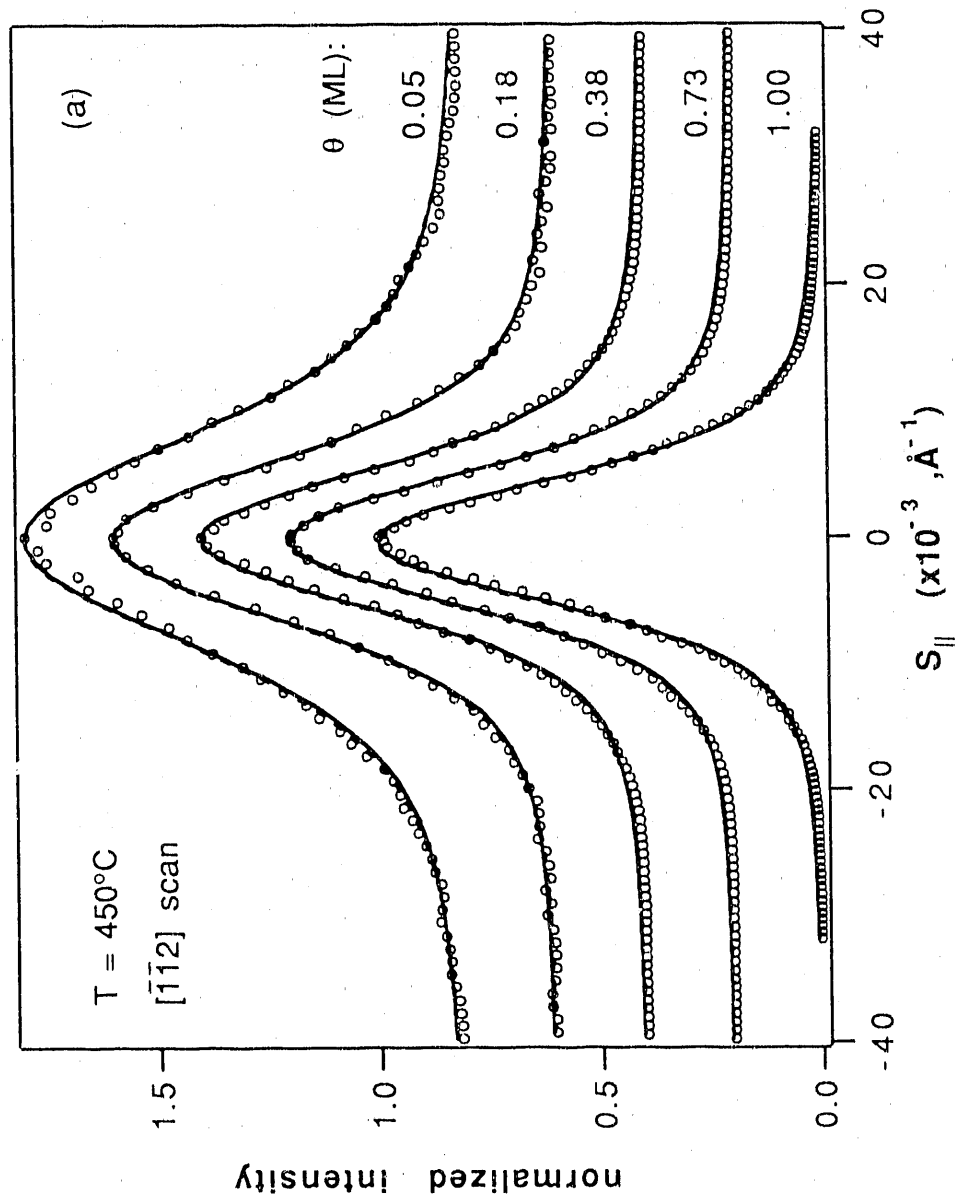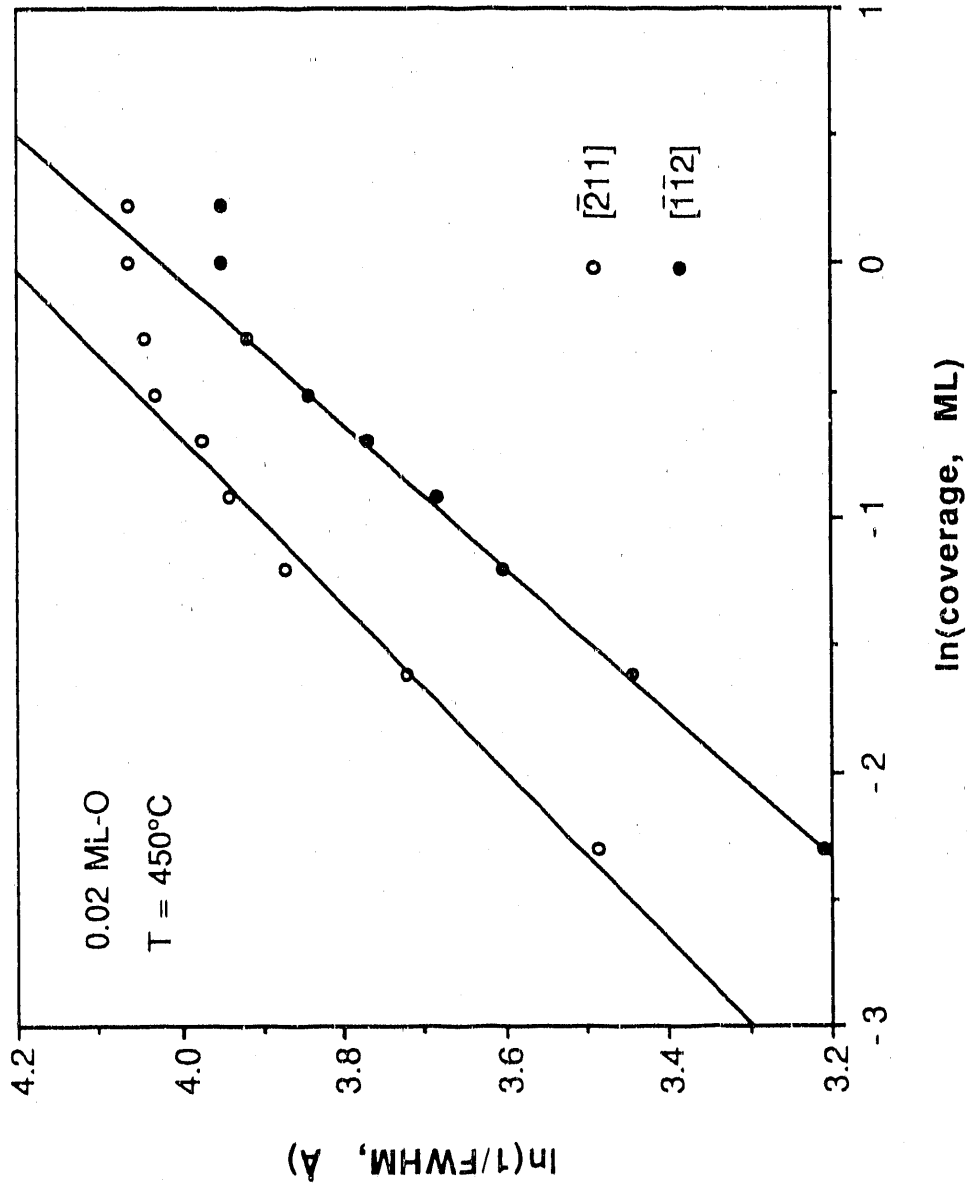
Fig. 5(b)

Fig. 6

END

DATE FILMED

11 / 08 / 90